Journal of Materials Chemistry A

Accepted Manuscript

This article can be cited before page numbers have been issued, to do this please use: W. Jiang, J. Hu, X. Zhang, Y. Jiang, B. Yu, Z. Wei and L. Wan, *J. Mater. Chem. A*, 2014, DOI: 10.1039/C4TA01780C.

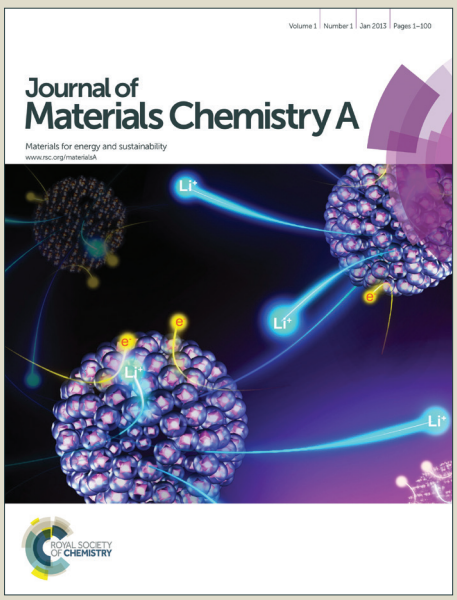

ROYAL SOCIETY OF CHEMISTRY

www.rsc.org/materialsA

View Article Online
DOI: 10.1039/C4TA01780C

Journal of Materials Chemistry A RSCPublishing

ARTICLE

In-situ nitrogen-doped nanoporous carbon nanocables as an efficient metal-free catalyst for oxygen reduction reaction

Wen-Jie Jiang,[a,b] Jin-Song Hu,*[a] Xing Zhang,[a] Yan Jiang,[a] Bin-Bin Yu,[a] Zi-Dong Wei,*[b] and Li-Jun Wan*[a]

Cite this: DOI: 10.1039/xoxxoooooox

Received ooth January 2012,
Accepted ooth January 2012

DOI: 10.1039/xoxxoooooox

www.rsc.org/

A new N-doped carbon nanomaterial with nanoporous coaxial nanocable structure was designed for achieving the requirements of high nitrogen content, proper nitrogen bonding state, and sufficient electron and mass transportation for an oxygen reduction reaction (ORR) catalyst. The nanoporous sheaths provided more catalytic sites and allowed oxygen and reactants to easily access them for fast mass transfer while carbon nanotube cores provided a three-dimensional conductive network and guaranteed fast electron transfer. As a result, the designed low-cost catalyst exhibited the excellent electrocatalytic performance and became one of most active metal-free ORR catalysts.

1. Introduction

Fuel cell, as a clean and efficient energy conversion device, is a promising technique in tackling future global energy crisis.[1, 2] However, the sluggish cathode oxygen reduction reaction (ORR) not only limits the performance but also relies on precious and scarce platinum group metals (PGM), which hampers the further development and genuinely practical application of this technology. Much progress has been made to reduce cost and improve performance of the catalysts by alloying PGM with transition metals,[3, 4] but it will still eventually encounter the cost problem on the way of commercialization. Therefore, extensive attentions gradually move to develop non-precious catalysts to replace commercial state-of-the-art Pt/C catalysts, including transition metal oxides,[5, 6] carbon materials doped with heteroatom,[7, 8] metal-N_4 structure catalysts,[9, 10] and their composites.[11, 12] Metal or metal oxide based catalysts usually have intrinsic issues like dissolution, sintering, and agglomeration during the operation of the fuel cell.[13] Doped carbon materials, as metal-free catalysts, are attractive options due to no these issues and the advantages of low cost and excellent resistance to methanol, especially for use in alkaline fuel cells.[14]

With the progress in tuning intrinsic property of carbon material with a series of heteroatoms, such as B,[15] N,[16, 17] S,[18] P,[19] plenty of doped carbon catalysts, including dual-doped [20, 21] and trinary-doped carbon materials,[22] had been reported although the catalytic mechanism still remain unrevealed.[23, 24] Among them, N-doping is most popular. In general, N-doped metal-free carbon catalysts are prepared mainly through three different routes. First route is in-situ introduction of nitrogen atom into carbon framework upon the formation of graphitic plane via processes like chemical vapor deposition (CVD).[25-27] This approach is often able to make high nitrogen content in carbon materials, but is not practicable for mass production of the catalysts for genuine application. Second one is post-heating graphitic carbon, including carbon nanotubes (CNTs), graphene and fullerene, with nitrogen-containing substances.[28-30] Because of incorporation resistance from pre-existing graphitic structure, the nitrogen fraction is usually too insufficient to make enough catalytic sites. The last approach is direct pyrolysis of nitrogen-rich precursors, such as graphitic carbon nitride,[31] melamine foam[32] and polymer framework.[33, 34] But the low electron conductivity of the materials obtained through this approach does not favor electrocatalytic process.

Although tremendous effort has been made, the design of cheap and stable catalysts for ORR is still a main challenge in this area. And to be viable, the activities of these catalysts should at least approach that of traditional but more expensive Pt/C catalysts. Therefore, the rational design of N-doped carbon materials as efficient metal-free ORR catalysts for practical application needs to meet several requirements: 1) high content of nitrogen in proper chemical bonding state to make as many catalytically active sites as possible for boosting activity; 2) sufficient electron conductivity to favor electron transfer, especially in practical fuel cell applications; and 3) easy access to catalytically active sites and fast mass transfer (ORR occurs at solid-liquid-gas three-phase-interface, which requires the reactants can easily access the active sites of catalysts).

Taking into account these requirements, we designed here a new N-doped carbon material with nanoporous coaxial nanocable structure as metal-free ORR catalyst. The nanoporous carbon sheath not only

View Article Online
DOI: 10.1039/C4TA01780C

imparts high surface area to the catalyst, but also allows the reactants to easily access the catalytically active sites and facilitates mass transfer. More importantly, the N-doping was in-situ achieved during the formation of nanopores at high temperature, which allow us to achieve high concentration of N-doping. The carbon nanotube cores provide a three-dimensional conductive network and guarantee the sufficient electron conductivity for fast electron transfer. Moreover, N-doping in high concentration on porous sheath instead of directly on carbon nanotube core will alleviate the damage of doping on carbon nanotube core and thus assure the good conductivity of the materials. As a result, the designed catalyst showed excellent electrocatalytic activity for ORR comparable to commercial Pt/C catalysts, as well as better durability and tolerance to methanol.

2. Experimental

Synthesis of CNT@NPC

All chemicals were of analytical grade purity and were used directly without further purification. Multi-walled CNTs (40-60 nm in diameter and 5-15 μm in length, Shenzhen Nanotech Port Co. Ltd.) were firstly refluxed in 6 M HNO_3 solution for 48h to remove metal and impurities and to make them dispersible in water. In a typical synthesis, 20 mg pretreated CNTs were ultrasonically dispersed in 10 ml of aqueous solution containing 800 mg glucose (Sinopharm Chemical Reagent Co., Ltd.) and 10 mg sodium dodecyl sulfate (SDS, Sinopharm Chemical Reagent Co., Ltd.). The black suspension was then transferred into an autoclave with 25 ml Teflon liner and heated at 180 °C for 15 h to produce precursor. After the reaction, the dark brown precursor was collected by centrifugation, washed with de-ionized water and ethanol, followed by drying at 60 °C overnight. The as-obtained solid product and melamine were ground together in a mass ratio of 1:10 to obtain a light gray mixture. This mixture was then put into a quartz tube under argon atmosphere and heated to certain temperature at a rate of 10 °C /min. After the pyrolysis at certain temperature for 2 h, the final product was cooled down naturally to room temperature and collected for characterization and electrochemical tests. The samples pyrolyzed at 800, 900, and 1000 °C are designated as CNT@NPC-800, CNT@NPC-900, and CNT@NPC-1000 respectively.

Characterization

The morphology of CNT@NPC samples was characterized by scanning electron microscope (JSM 6701, JEOL, Japan) operating at 10 kV and transmission electron microscopy (Tecnai F20 X-Twin microscope, FEI, USA) working at an accelerating voltage of 200 kV. X-ray photoelectron spectroscopy measurements were performed on a VG ESCALab220i-XL using a monochromic Mg Kα source. Nitrogen adsorption-desorption isotherms were measured on Quantachrome Autosorb AS-1 at 77 K. Before measurements, the samples were degassed in a vacuum at 150 °C for at least 6 h.

Electrochemical tests

The glass carbon rotating disk electrode (RDE, 3 mm in diameter, INF-EL-EDI101, France Radiometer Analytical S.A.) was polished mechanically prior to use with 0.5~0.7 μm and then down to 0.03~0.05 μm alumina slurry to obtain a mirror-like surface, followed by washing with Mill-Q water and ethanol, and then dry in air. In a typical procedure for ink preparation, 2 mg catalysts were dispersed in 400 μL ethanol and sonicated for 30 minutes to form a homogeneous ink. 5 μL ink was loaded on polished glassy carbon electrode to achieve a catalyst loading of 0.354 mg/cm^2. A drop of 0.5 wt. % nafion (Sigma-Aldrich) solution was then applied onto on the surface of catalysts. After drying in the air, the electrode was ready for test. Commercial Johnson-Matthey Pt/C with 20 wt.% Pt loading was used for comparison. The loading of Pt/C catalyst was 0.127 mg/cm$^2_{Pt+C}$.

Electrochemical experiments were conducted in a standard three-electrode cell at room temperature on PARSTAT 2273 advanced electrochemical system. The cell consisted of a working electrode with catalyst, Ag/AgCl reference electrode and a platinum foil as counter electrode. All the CV measurements were done at a scan rate of 50 mV/s. The polarization curves were recorded in O_2-saturated 0.1 M KOH at a scan rate of 10 mV/s. Before each test, the electrolyte was purged with O_2 for at least 30 min to achieve O_2 saturated solution. RDE measurements were conducted at different rotating speeds from 400 to 3600 rpm by using CTV101 Speed Control Unit (France Radiometer Analytical S.A.).

Calculation for electron transfer number

The electron transfer number per oxygen molecule involved in ORR were calculated from the slopes of Koutecky-Levich plots by using the following equation:[S1]

$$\frac{1}{j} = \frac{1}{j_k} + \frac{1}{B\omega^{1/2}}$$

Where j_k is the kinetic current and ω is the electrode rotating rate. B could be determined from the slope of the K-L plots based on the Levich equation as follows:

$$B = 0.62nF(D_0)^{2/3}\vartheta^{-1/6}C_0$$

Where n represents the electron transfer number, F is the Faraday constant ($F = 96485\ C\ mol^{-1}$), D_0 is the diffusion coefficient of O_2 in 0.1 M KOH ($1.9 \times 10^{-5} cm^2\ s^{-1}$), ϑ is the kinetic viscosity ($0.01\ cm^2\ s^{-1}$), and C_0 is the bulk concentration of O_2 ($1.2 \times 10^{-6} mol\ cm^{-3}$). The constant of 0.62 is adopted when the rotating speed is expressed in $rad\ s^{-1}$.

3. Results and discussion

As shown in Fig. 1a, the cable-like materials composed of CNT cores and N-doped porous carbon shells (labelled as CNT@NPC) were synthesized by first hydrothermally coating CNTs with carbonaceous sheath, followed by the formation of nanopores in shells and in-situ doping the materials with nitrogen. In brief, CNTs were first controllably coated with a carbonaceous layer via glucose polymerization reaction under hydrothermal condition. In order to achieve cable-like sheath on the outer surfaces of CNTs, the as-received CNTs was pre-treated with acid to functionalize the CNT surfaces for inducing on-surface polymerization reaction and improve the dispersion of CNTs in aqueous solution. The product was then mixed with nitrogen-rich doping source (melamine). During the following heat treatment at certain temperature, the pyrolysis of carbonaceous layer generated plenty of nanopores in shells due to the volatilization of small organic moieties and rearrangement of carbon atoms at high temperature. Simultaneously, nitrogen-rich melamine decomposed to

J Mater. Chem. A

View Article Online
DOI: 10.1039/C4TA01780C

generate nitrogen species, which involved in the reaction and rearrangement of carbon atoms and formed N-doped porous carbonized layer. It should be noted that there is possibility that the nitrogen species could also diffuse onto and dope the inner CNT cores. But in view of the facts that the pyrolysis of carbonaceous layer and rearrangement of carbon atoms in shells were occurring simultaneously outside CNT cores during the N-doping and the N species were diffusing from outside, it could be speculated that most of N-doping would likely take place in the shells. Since the N-doping and the formation of porous carbonized shells with high surface area were achieved at the same time, the higher nitrogen content could be achieved in the product, compared to that through other post-doping methods.[31, 35]

The morphology of the product was first investigated by scanning electron microscopy (SEM) and transmission electron microscopy (TEM). The typical SEM image (Fig. 1b) shows that the product after hydrothermal coating process maintains the morphologies similar to CNTs with smooth surfaces except for a larger average diameter (ca. 150 nm *vs.* 50 nm), implying the successful and uniform coating of carbonaceous layer on CNTs. The TEM image in Fig. 1c evidences that the product has coaxial cable-like structures. The inner part can be attributed to CNTs. The apparent image contrast difference between inner and outer parts clearly reveals that the entire surfaces of all CNTs are uniformly coated with a ca. 50 nm thick sheath. After the pyrolysis at 900 ºC, SEM image in Fig. 1d shows that the morphology of the product (designated as CNT@NPC-900) does not change much except for the shrinked diameter, which can be ascribed to the decomposition and gasification of organic component in carbonaceous sheath. TEM image in Fig. 1e confirms that the carbonized sheath became thinner (ca. 25 nm vs. 50 nm) and unifomly coated on the entire outer surface of CNTs. The slightly light image contrast in sheath part implies that this layer does not have fully graphitized structure like CNTs. High resolution TEM image in Fig. 1f clearly reveals the lattice fringes in inner part with a distance of ca 0.34 nm matching well with the interplanar distance of (002) planes of CNTs, as well as somewhat disordered outer sheath, corresponding to the carbonized coating layer. In order to invesigate the effect of pyrolysis temperature on the morphologies and performance of the products, the products were also pyrolyzed at 800 and 1000 ºC, and designated as CNT@NPC-800 and CNT@NPC-1000 hereinafter, respectively. As shown in Fig. S1, the SEM and TEM observation suggests all products presented similar morphologies and structures except for a slight thickness shift in sheath layer (30-40 nm for CNT@NPC-800 and 10-20 nm for CNT@NPC-1000), which is consistent with the change of pyrolysis temperature. It is also interestingly noted that the ends of many CNTs in all three samples did not fully coated with carbon layer and CNT tips exposed, as marked in orange circles in Fig. 1c and Fig. S2. These exposed CNT tips could enhance the role of three-dimensional conductive network of CNTs in catalysts and facilitate the electron migration.

The surface area and porosity are important parameters for ORR catalysts since high surface area would provide more catalytic sites and high porosity would benefit the mass transfer. Therefore, the surface area and porosity of the products were further characterized by nitrogen isothermal adsorption technique. The adsorption-desorption isotherms of sample CNT@NPC-900 shown in Fig. 1g exhibits a typical hysteresis of a nanoporous system, indicating these nanocables contain

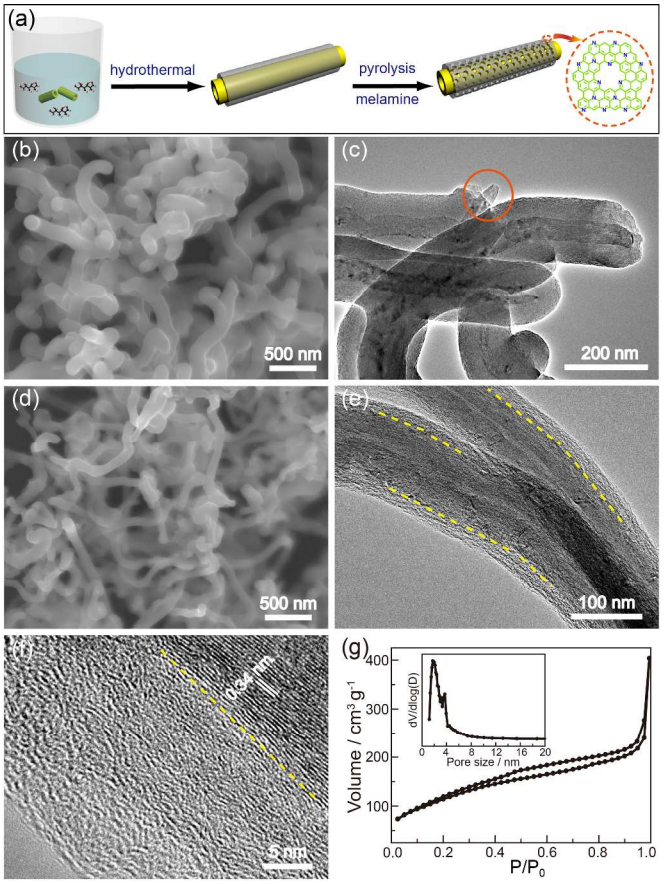

Fig. 1 (a) Schematic illustration of the preparation of the nanoporous coaxial carbon nanocables. (b) Typical SEM and (c) TEM images of the product before pyrolysis. (d) Typical SEM, (e) TEM and (f) HRTEM images of the product after pyrolysis at 900 °C (CNT@NPC-900). (g) N_2 adsorption-desorption isotherm of CNT@NPC-900. Inset is the plot of BJH pore size distribution.

nanoporous structures. The total specific surface area according to Brunauer-Emmett-Teller (BET) analysis is 413 m^2/g, which is much larger than that of pristine acid-treatment CNTs of 79.5 m^2/g (Fig. S3a). The dramatic increase in surface area can only be ascribed to the porous carbon sheath. The Barrett-Joyner-Halenda (BJH) pore size distribution analysis (inset in Fig. 1g) reveals that the diameters of most pores in the sheath lie in the range from 1.7 nm to 4 nm, which should be large enough for free diffusion of oxygen molecules with a kinetic diameter of 0.34 nm.[36] The data of BET analysis of sample CNT@NPC-800 and CNT@NPC-1000 were summarized in Table 1 and Fig. S3. It can be seen that BET surface area was dramatically enhanced by ~4 fold (79.5 *vs.* 413 m^2/g) when the pyrolysis temperature increased from 800 ºC to 900 ºC, and slightly increased as temperature further increased to 1000 ºC.

It was reported that the nitrogen content and chemical bonding state play an important role in electrocatalytic activity of N-doped catalysts for ORR.[17, 24, 37, 38] X-ray photoelectron spectroscopy (XPS) measurements were performed to determine the composition of the as-produced N-doped CNT@NPCs and analyze the bonding state of nitrogen in each sample. As presented in Fig. 2a, XPS spectra recorded on all three samples exhibit obvious N signals, confirming that nitrogen was successfully introduced into the product. No signals of other elements in full scan range demonstrate the catalysts are free of metal.

View Article Online
DOI: 10.1039/C4TA01760C
Article

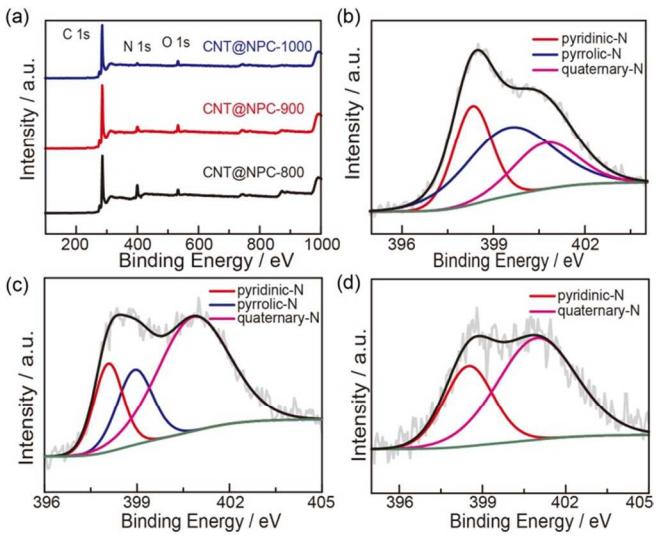

Fig. 2 (a) Wide-scan survey XPS spectra of the three CNT@NPCs. (b, c, d) High-resolution N 1s peaks in XPS spectra of CNT@NPC-800, CNT@NPC-900 and CNT@NPC-1000, respectively.

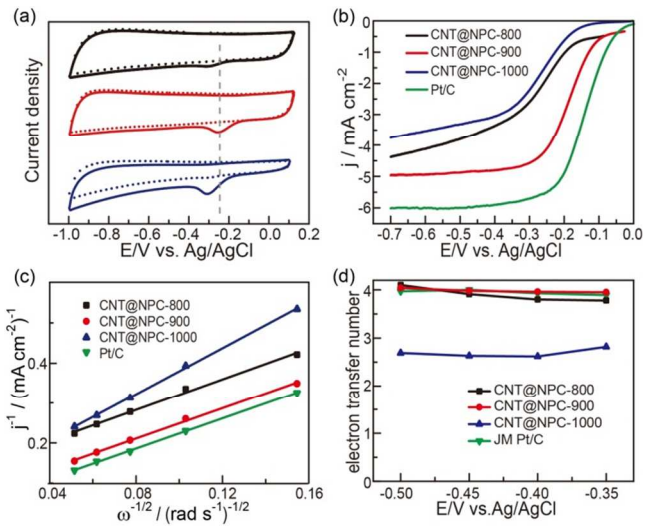

Fig. 3 (a) CVs of CNT@NPC-800 (black), -900 (red), -1000 (blue) in N_2-saturated (dotted line) and O_2-saturated (solid line). (b) Polarization curves recorded in O_2-saturated 0.1 M KOH at a scan rate of 10 mV s^{-1} and rotation speed of 1600 rpm. (c) Koutecky-Levich plots at -0.45 V. (d) Electron transfer numbers at various potential of different samples.

Moreover, it can be seen that the intensity of nitrogen signal decreases significantly when the pyrolysis temperature reaches 1000 ºC, implying the appreciable decrease in nitrogen content. The quantitative analysis listed in Table 1 reveals that the nitrogen content in CNT@NPC-800 is as high as 15.76%, which is the highest values reported for N-doped carbon catalysts,[36] to our best knowledge. Even pyrolyzed at 900 °C, the sample CNT@NPC-900 still has 6.93% nitrogen, higher than other N-doped carbon materials (2~5%).[31, 35] The achievement of high nitrogen content can be attributed to the synchronous and in-situ N-doping during the formation of nanoporous carbon sheath with high surface area. The fact that the higher pyrolysis temperature the less nitrogen remained in the sample is reasonable since the more organic moieties and melamine (nitrogen source) will be decomposed and evaporated at higher temperature. Furthermore, by comparing the high-resolution N 1s peaks of three samples shown in Fig. 2b-d, it can be seen that the shapes of peaks are apparently different; indicating the bonding states of nitrogen are different in three samples. In order to further investigate the bonding state of nitrogen, the N 1s signals in each spectrum were well deconvoluted into the components corresponding to pyridinic type, pyrrolic type, and quaternary type nitrogen. The binding energy for each type of N was selected according to the previous reports[24] and summarized in Table S1. The result of quantitative analysis summarized in Table 1 clearly reveals that pyrrolic-N dominates in sample CNT@NPC-800, but quaternary-N dominates in sample CNT@NPC-900 and CNT@NPC-1000.

Table 1 BET surface areas and nitrogen contents calculated from XPS spectra for pristine CNTs and CNT@NPCs.

Sample	SA[a]	N[b]	N1[c]	N2[d]	N3[e]
pristine CNTs	79.5	-	-	-	-
CNT@NPC-800	101	15.76	29.6	46.9	23.5
CNT@NPC-900	413	6.93	18.9	20.1	61.0
CNT@NPC-1000	479	3.54	32.9	-	67.1

[a] Surface area (m^2 g^{-1}) from BET measurement. [b] Nitrogen content (at.%) calculated from XPS measurement. [c, d, e] Fraction (%) of pyridinic-N (N1), pyrrolic-N (N2) and quaternary-N (N3), respectively, calculated from deconvoluted high-resolution N1s spectra. '-' indicates 'not detectable'.

The electrocatalytic performance of N-doped nanoporous carbon nanocables was firstly evaluated by carrying out three-electrode cyclic voltammetry (CV) experiments in O_2-free and O_2-saturated 0.1 M KOH solution at a scan rate of 50 mV s^{-1}. Comparing to the featureless CV curves recorded in N_2-saturated (O_2-free) solution (dotted line), distinct ORR peaks recorded in O_2-saturated electrolyte suggested that all the catalysts are active for oxygen reduction (Fig. 3a). The ORR onset potential for CNT@NPC-900 was about -0.114 V (*vs*. Ag/AgCl, all potential will be relative to Ag/AgCl unless specifically illustrated hereinafter), which is more positive than that for CNT@NPC-800 and CNT@NPC-1000, indicating better activity for ORR. The electrocatalytic activities for ORR of three samples were further investigated via linear sweep voltammetry (LSV) experiments by using a rotating disk electrode (RDE) and compared to commercial Johnson Matthey (JM) Pt/C catalysts (20 wt.% Pt loading). As shown in Fig. 3b, CNT@NPC-900 showed the best performance with the most positive half-wave potential ($E_{1/2}$, *viz.* a potential at which the current is half of the limiting current in LSV curve, which was commonly used to assess ORR catalysts) of -0.184 V. In comparison with the half-wave potential of 20% Pt/C at -0.142 V, this value is only 42 mV negative. It should be noted that the minimum activity requirement for non-Pt electrocatalysts for possible replacement of platinum is that the non-Pt catalysts should have activity at 0.800 V (vs. RHE) comparable to Pt catalysts at 0.900 V (vs. RHE) under the condition that catalyst layer on electrode is not too thick.[39] This is the reason why most Pt-free catalysts are evaluated at -0.2 V *vs*. Ag/AgCl in 0.1 M KOH solution. Therefore, the present catalyst was evaluated at this potential. It can be seen that the mass current density for CNT@NPC-900 at -0.2 V reached 8.43 mA/mg, closed to 11.9 mA/mg_{Pt+C} for commercial 20% Pt/C at -0.1 V. Table S2 also summarized the electrocatalytic performance of metal-free nitrogen-doped catalysts recently reported in literatures. It can be seen that the present CNT@NPC-900 catalyst is most active for ORR in terms of more positive onset potential and half-wave potential. These

J Mater. Chem. A

View Article Online
DOI: 10.1039/C4TA01760C Article

results show that the present catalyst of CNT@NPC-900 showed the excellent electrocatalytic performance for ORR and can potentially be used as a Pt-free catalyst candidate for fuel cell applications.

On the other hand, it is noted that CNT@NPC-900 showed much better ORR activity than the other two samples (CNT@NPC-800 and CNT@NPC-1000), which could be justified by the nitrogen doping level and the activity difference in different types of nitrogen species. It has been reported that the nitrogen content in N-doped carbon materials is positively related to their ORR activity; and the quaternary-N and pyridinic-N are more active than pyrrolic-N for ORR.[24, 37, 38] Since the nitrogen content in CNT@NPC-900 is almost two times than that in CNT@NPC-1000 (6.93% vs. 3.54%), the former exhibited better ORR activity. Although the nitrogen content in CNT@NPC-800 is highest, the fraction of more active nitrogen species is much lower than that in CNT@NPC-900 as shown in Table 1. The surface area and pore volume of CNT@NPC-800 are one-fifth and three-fifth that of CNT@NPC-900 indicates the less exposed catalytically active sites and the worse mass transfer in the former. The pore volume is 0.272 cc/g for CNT@NPC-800, and 0.443 cc/g for CNT@NPC-900. Plus taking into account the possibly worse conductivity of porous carbon sheath due to the less graphitization at lower temperature, CNT@NPC-800 exhibited the worse ORR activity than CNT@NPC-900.

To give further insight into the electron transfer process in ORR catalyzed by the studied catalysts, we carried out a serial of LSV measurements on three samples at different rotating speeds of RDE (Fig. S4). Fig. 3c presented the Koutecky-Levich (K-L) plots at -0.45V calculated from LSV curves at various rotating speeds based on Koutecky-Levich equation (see Supplementary Information for details). The K-L lines for CNT@NPC-900 and CNT@NPC-800 are in parallel with that for Pt/C, implying that ORR occurs on them in a similar way as that on Pt/C. Accurate electron transfer numbers (n) at various potentials were calculated through K-L equation and plotted in Fig. 3d. It can be inferred that ORR takes place on CNT@NPC-900 catalyst in more efficient and beneficial four- electron (4e) reaction pathway, while in a combined pathway of 2e and 4e reductions on CNT@NPC-1000 catalyst.

It should be noted that the ratios of CNTs, porous carbon sheath precursor (glucose) and nitrogen-rich precursor (melamine) used in the preparation of catalysts will also affect the activities of catalysts. First, the influence of the ratio of CNTs and porous carbon sheath precursor (glucose) on the electrocatalytic performance of final CNT@NPC catalysts was evaluated. Three catalysts were prepared in parallel at the same conditions as that for CNT@NPC-900 except for the different mass ratios of CNTs and glucose in hydrothermal processing (1:20, 1:40, and 1:80). This change affected the thickness of the nanoporous carbon sheath. TEM images in Fig. 4a, 4b, and 1e show that the thicknesses of the carbonized porous sheath are ~9 nm, ~25nm and ~65 nm for the catalysts prepared at the ratio of 1:20, 1:40 (Fig. 1e) and 1:80, respectively. The polarization curves of these three catalysts shown in Fig. 4c indicated that the catalyst prepared at the ratio of 1:40 had more positive on-set potential and half-wave potential and thus better catalytic activity than other two catalysts. The inferior activity for the catalyst (1:20) could be because the thinner nanoporous sheath with lower surface area provided the less amount of sites for N-doping and thus produced less catalytic sites for ORR. On the other hand, if the sheath was too thick like situation in the catalyst (1:80), the electron

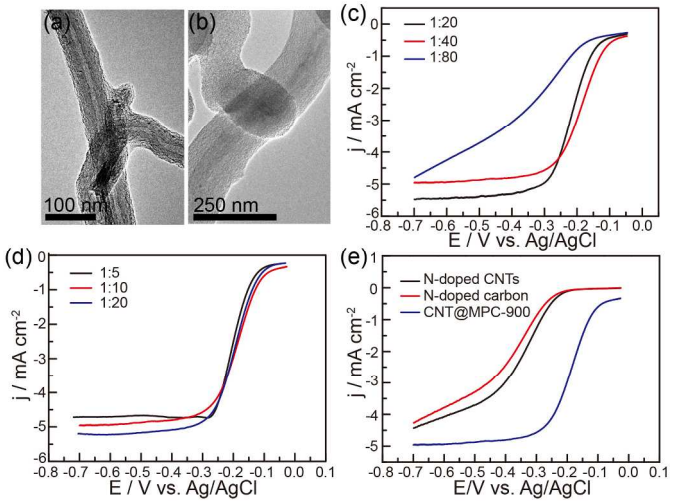

Fig. 4 (a-b) Typical TEM images of the catalysts prepared at different mass ratios of CNTs and glucose in hydrothermal processing: (a) 1:20, (b) 1:80. (c) Polarization curves of catalysts prepared at different mass ratios of CNTs and glucose. (d) Polarization curves of catalysts prepared at different mass ratios of CNT@NPC precursor and melamine. (e) The comparison of electrochemical performances of N-doped CNTs, N-doped carbon and CNT@MPC-900. All curves were recorded in O_2-saturated 0.1 M KOH at a scan rate of 10 mV s^{-1} and rotation speed of 1600 rpm. The catalyst loadings are 0.354 mg cm^{-2}.

transport via conductive CNT core would not be efficient since the electron conductivity of the nanoporous sheath was much worse than that of CNT core. This speculation was consistent with the results implied by the shapes of polarization curves in Fig. 4c. Therefore, 1:40 was chosen as the mass ratio of CNTs and nitrogen-free precursor (glucose). Seond, the influence of the ratio of CNT@NPC precursor (the product of the hydrothermal process) and nitrogen-rich precursor (melamine) was further investigated. Three catalysts prepared in parallel at the same conditions as that for CNT@NPC-900 except for the different mass ratios of CNT@NPC precursor and melamine (1:5, 1:10, and 1:20) were evaluated. The polarization curves of these three catalysts shown in Fig. 4d indicated that the catalyst (1:10) had more positive on-set potential and half-wave potential and thus better catalytic activity than the catalyst (1:5). This could be because the less amount of nitrogen-rich precursor led to the insufficient N-doping and thus the less amount of catalytically active sites for ORR. The activity of the catalyst (1:10) was comparable to the catalyst (1:20). In the consideration of using less chemicals for low cost, 1:10 was chosen as the mass ratio of CNT@NPC precursor and melamine.

Furthermore, in order to further demonstrate the advantages of the designed CNT@NPC catalysts with nanoporous sheath and conductive CNT cores, two more control catalysts were prepared in parallel at the same conditions as that for CNT@NPC-900. One is pure N-doped CNTs without nanoporous sheath. The other is N-doped carbon from glucose polymerization and N-doping with no addition of CNTs. Fig. 4e shows the comparison of ORR electrocatalytic performances of these two catalysts and CNT@NPC-900. It can be clearly seen that the designed CNT@NPC-900 catalysts exhibited much enhanced electrocatalytic activity for ORR in terms of impressively positive shift of on-set potential and half-wave potential.

Moreover, fuel crossover is an important issue in fuel cells.[19] A good ORR catalyst should exhibit satisfactory tolerance to fuel, for example

View Article Online
DOI: 10.1039/C4TA01786C
Article

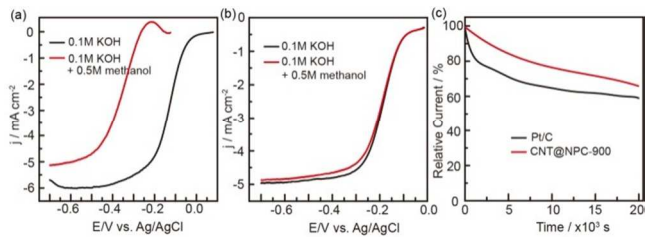

Fig. 5 RDE polarization curves of Pt/C (a) and CNT@NPC-900 (b) in O_2-saturated 0.1 M KOH in the presence or absence of 0.5 M methanol. (c) Current-time (i-t) chronoamperometric responses of CNT@NPC-900 and Pt/C at -0.2 V in O_2-saturated 0.1 M KOH at a rotation rate of 1600rpm.

methanol in direct methanol fuel cells. Therefore, we measured the polarization curves of both CNT@NPC-900 and Pt/C catalysts in the presence or absence of 0.5 M methanol for testing possible poisoning effects. As seen in Fig. 5a, a severe negative shift was found for LSV curve of Pt/C catalyst recorded in the presence of 0.5 M methanol. The drastic negative shift of $E_{1/2}$ of 214 mV indicated the dramatic decrease of ORR activity in the presence of methanol. In contrast, almost no loss in $E_{1/2}$ was observed in case of CNT@NPC-900 (Fig. 5b), revealing that it exhibited excellent tolerance to methanol poisoning effects. Lastly, the durability of the catalysts was checked by chronoamperometric technique. It can be seen in Fig. 5c that the commercial Pt/C suffered from a 40% decrease in current density after 20000s test while CNT@NPC-900 showed only about 30% loss, suggesting CNT@NPC-900 had better durability.

4. Conclusions

In summary, we have described a simple method to successfully synthesize a new type of N-doped nanocable-type carbon materials as metal-free ORR catalysts. The materials are composed of CNT cores and N-doped nanoporous carbon shells. CNT core plays a role of a three-dimensional conductive network for fast electron transfer. N-doped nanoporous shell brings more catalytically active sites and fast mass transfer for ORR. As indicated by the onset potential of -0.114 V, the half-wave potential of -0.184 V, the limit current density of 5 mA/cm^2, and the mass current density of 8.43 mA/mg at -0.2 V at rotation speed of 1600 rpm, as well as good durability and tolerance to methanol, the designed CNT@NPC-900 catalyst has demonstrated the excellent electrocatalytic performance for ORR and is one of most active metal-free catalysts. The reported design idea could also inspire the development of similar electrocatalysts with even more better performance.

Acknowledgements

We gratefully acknowledge the support from the National Key Project on Basic Research (Grants No. 2011CB808700, and 2012CB215500), the National Natural Science Foundation of China (Grants Nos. 91127044, 21173237, and 21121063), and the Chinese Academy of Sciences.

Notes and references

[a] Beijing National Laboratory for Molecular Sciences, Key Laboratory of Molecular Nanostructure and Nanotechnology, Institute of Chemistry, Chinese Academy of Science, 2 North 1st Street, Zhongguancun, Beijing 100190, China. Email. hujs@iccas.ac.cn, wanlijun@iccas.ac.cn

[b] State Key Laboratory of Power Transmission Equipment & System Security and New Technology, College of Chemistry and Chemical Engineering, Chongqing University, Chongqing 400044, China. Email. zdwei@cqu.edu.cn

† Electronic Supplementary Information (ESI) available: synthesis, characterization and electrochemical tests of the catalysts. See DOI: 10.1039/c000000x/

1. H. A. Gasteiger and N. M. Marković, *Science*, 2009, **324**, 48-49.
2. M. K. Debe, *Nature*, 2012, **486**, 43-51.
3. D. Wang, H. L. Xin, R. Hovden, H. Wang, Y. Yu, D. A. Muller, F. J. DiSalvo and H. D. Abruna, *Nat. Mater.*, 2013, **12**, 81-87.
4. V. R. Stamenkovic, B. Fowler, B. S. Mun, G. Wang, P. N. Ross, C. A. Lucas and N. M. Marković, *Science*, 2007, **315**, 493-497.
5. J. Suntivich, H. A. Gasteiger, N. Yabuuchi, H. Nakanishi, J. B. Goodenough and Y. Shao-Horn, *Nat. Chem.*, 2011, **3**, 546-550.
6. H. Zhu, S. Zhang, Y.-X. Huang, L. Wu and S. Sun, *Nano Lett.*, 2013, **13**, 2947-2951.
7. K. Gong, F. Du, Z. Xia, M. Durstock and L. Dai, *Science*, 2009, **323**, 760-764.
8. Y. Li, W. Zhou, H. Wang, L. Xie, Y. Liang, F. Wei, J.-C. Idrobo, S. J. Pennycook and H. Dai, *Nat. Nanotechnol.*, 2012, **7**, 394-400.
9. M. Lefèvre, E. Proietti, F. Jaouen and J.-P. Dodelet, *Science*, 2009, **324**, 71-74.
10. G. Wu, K. L. More, C. M. Johnston and P. Zelenay, *Science*, 2011, **332**, 443-447.
11. Y. Liang, Y. Li, H. Wang, J. Zhou, J. Wang, T. Regier and H. Dai, *Nat. Mater.*, 2011, **10**, 780-786.
12. Z.-S. Wu, S. Yang, Y. Sun, K. Parvez, X. Feng and K. Müllen, *J. Am. Chem. Soc.*, 2012, **134**, 9082-9085.
13. Y.-J. Wang, D. P. Wilkinson and J. Zhang, *Chem. Rev.*, 2011, **111**, 7625-7651.
14. L. James and D. Andrew, *Fuel Cell Systems Explained*, John Wiley & Sons, 2003.
15. L. Yang, S. Jiang, Y. Zhao, L. Zhu, S. Chen, X. Wang, Q. Wu, J. Ma, Y. Ma and Z. Hu, *Angew. Chem. Int. Ed.*, 2011, **50**, 7132-7135.
16. Q. Li, S. Zhang, L. Dai and L.-s. Li, *J. Am. Chem. Soc.*, 2012, **134**, 18932-18935.
17. R. Silva, D. Voiry, M. Chhowalla and T. Asefa, *J. Am. Chem. Soc.*, 2013, **135**, 7823-7826.
18. Z. Yang, Z. Yao, G. Li, G. Fang, H. Nie, Z. Liu, X. Zhou, X. a. Chen and S. Huang, *ACS Nano*, 2011, **6**, 205-211.
19. D.-S. Yang, D. Bhattacharjya, S. Inamdar, J. Park and J.-S. Yu, *J. Am. Chem. Soc.*, 2012, **134**, 16127-16130.
20. J. Liang, Y. Jiao, M. Jaroniec and S. Z. Qiao, *Angew. Chem. Int. Ed.*, 2012, **51**, 11496-11500.
21. Y. Zheng, Y. Jiao, L. Ge, M. Jaroniec and S. Z. Qiao, *Angew. Chem. Int. Ed.*, 2013, **52**, 3110-3116.
22. S. Wang, L. Zhang, Z. Xia, A. Roy, D. W. Chang, J.-B. Baek and L. Dai, *Angew. Chem. Int. Ed.*, 2012, **51**, 4209-4212.
23. Y. Zhao, L. Yang, S. Chen, X. Wang, Y. Ma, Q. Wu, Y. Jiang, W. Qian and Z. Hu, *J. Am. Chem. Soc.*, 2013, **135**, 1201-1204.
24. L. Lai, J. R. Potts, D. Zhan, L. Wang, C. K. Poh, C. Tang, H. Gong, Z. Shen, J. Lin and R. S. Ruoff, *Energy Environ. Sci.*, 2012, **5**, 7936-7942.

J Mater. Chem. A View Article Online DOI: 10.1039/C4TA01780C Article

25. D. Wei, Y. Liu, Y. Wang, H. Zhang, L. Huang and G. Yu, *Nano Lett.*, 2009, **9**, 1752-1758.
26. A. L. M. Reddy, A. Srivastava, S. R. Gowda, H. Gullapalli, M. Dubey and P. M. Ajayan, *ACS Nano*, 2010, **4**, 6337-6342.
27. Z. Jin, J. Yao, C. Kittrell and J. M. Tour, *ACS Nano*, 2011, **5**, 4112-4117.
28. X. Wang, X. Li, L. Zhang, Y. Yoon, P. K. Weber, H. Wang, J. Guo and H. Dai, *Science*, 2009, **324**, 768-771.
29. Z.-H. Sheng, L. Shao, J.-J. Chen, W.-J. Bao, F.-B. Wang and X.-H. Xia, *ACS Nano*, 2011, **5**, 4350-4358.
30. F. Gao, G.-L. Zhao, S. Yang and J. J. Spivey, *J. Am. Chem. Soc.*, 2012, **135**, 3315-3318.
31. Y. Zheng, Y. Jiao, J. Chen, J. Liu, J. Liang, A. Du, W. Zhang, Z. Zhu, S. C. Smith, M. Jaroniec, G. Q. Lu and S. Z. Qiao, *J. Am. Chem. Soc.*, 2011, **133**, 20116-20119.
32. J.-S. Lee, G. S. Park, S. T. Kim, M. Liu and J. Cho, *Angew. Chem. Int. Ed.*, 2013, **52**, 1026-1030.
33. Y. Zhao, K. Watanabe and K. Hashimoto, *J. Am. Chem. Soc.*, 2012, **134**, 19528-19531.
34. M. Zhong, E. K. Kim, J. P. McGann, S.-E. Chun, J. F. Whitacre, M. Jaroniec, K. Matyjaszewski and T. Kowalewski, *J. Am. Chem. Soc.*, 2012, **134**, 14846-14857.
35. H. Wang, T. Maiyalagan and X. Wang, *ACS Catal.*, 2012, **2**, 781-794.
36. D. Deng, X. Pan, L. Yu, Y. Cui, Y. Jiang, J. Qi, W.-X. Li, Q. Fu, X. Ma, Q. Xue, G. Sun and X. Bao, *Chem. Mater.*, 2011, **23**, 1188-1193.
37. T. Sharifi, G. Hu, X. Jia and T. Wågberg, *ACS Nano*, 2012, **6**, 8904-8912.
38. K. Ai, Y. Liu, C. Ruan, L. Lu and G. Lu, *Adv. Mater.*, 2013, **25**, 998-1003.
39. H. A. Gasteiger, S. S. Kocha, B. Sompalli and F. T. Wagner, *Appl. Catal. B*, 2005, **56**, 9-35.

View Article Online
DOI: 10.1039/C4TA01780C